Colloid Polym Sci (2014) 292:3291–3299
DOI 10.1007/s00396-014-3378-6

ORIGINAL CONTRIBUTION

Energy dissipation in concentrated monodisperse colloidal suspensions of silica particles in polyethylene glycol

Mathieu Soutrenon · Véronique Michaud

Received: 22 November 2013 / Revised: 22 July 2014 / Accepted: 18 August 2014 / Published online: 5 September 2014

Abstract Highly concentrated colloidal suspensions exhibit a discontinuous shear-thickening behaviour. The transition from a low to a high viscosity state is associated to a large energy dissipation. This effect could find applications in structural damping while the viscosity increase brings added stiffness. In the present work, highly concentrated suspensions of monodisperse spherical silica particles in polyethylene glycol were selected for their strong thickening at low critical shear rates. Their damping properties were characterized by measuring the energy dissipated per cycle at low frequency (below 2 Hz) during oscillatory tests using a rheometer. The influence of parameters such as particle concentration, size and frequency was investigated. Damping was found to overcome that of benchmark elastomeric materials only in high frequencies and high strain domains.

Keywords Shear-thickening fluids · STF · Dissipated energy · Damping

Introduction

Shear-thickening fluids (STF) are non-Newtonian fluids that exhibit an increase in viscosity by several orders of magnitude, instantly and reversibly, under an imposed deformation field, at a critical shear rate. Several colloidal suspensions have been reported to behave as shear thickening fluids, including starch in water, and silica in polyethylene glycol [1, 2]. In particular, highly concentrated stabilized suspensions of monodisperse spherical silica particles in polyethylene glycol exhibit a large discontinuous shear thickening effect [3, 4].

Shear thickening behaviour in colloidal suspensions relies on the formation of agglomerates of particles, known as hydroclusters. This name originated from the fact that clusters are formed by hydrodynamic forces. At rest or low strain rates, particles in suspensions tend to move away from each other due to repulsive interparticle electrostatic or Brownian forces, which stabilize the suspension, and maintain a low viscosity [5]. With an increase of the flow rates, hydrodynamic forces increase, and tend to move the particles closer. When the hydrodynamic lubrication forces become higher than the repulsive forces, the particles aggregate into clusters [6]. These aggregates limit flow and explain the strong increase of viscosity observed at a critical shear rate. When hydrodynamic forces decrease, hydroclusters break up and the viscosity goes back down. The fundamentals of hydroclustering theory have been first exposed for spherical Brownian suspensions in function of the Peclet number [6]. For the low-shear structure, the shear viscosity was shown to be proportional to the Peclet number [7]. Hydroclusters have been observed by combined rheology and optical measurements [8] or small-angle neutron scattering [9].

The rheological properties of shear thickening colloidal suspensions have been widely investigated for several types of STF [1, 10]. In general, their behaviour is extremely sensitive to variation of parameters including the viscosity of the fluid, the particle concentration or the size of the particles [1, 9, 11, 12]. As an example, a suspension of spherical silica particles of 500-nm diameter in polyethylene glycol with a molecular weight of 200 g mol $^{-1}$(PEG 200) displays discontinuous shear thickening properties only within

M. Soutrenon · V. Michaud (✉)
Laboratoire de Technologie des Composites et Polymères (LTC) Ecole Polytechnique Fédérale de Lausanne (EPFL), 1015 Lausanne, Switzerland
e-mail: veronique.michaud@epfl.ch

a narrow range of particle concentration between 67 and 68 % *w/w* [11]. Shear thickening is a non-linear response of the fluid triggered by large deformation or high stresses that remains difficult to characterize using conventional rheological procedures at low frequencies and deformation. In consequence, recent research related to STF extended their characterization with large amplitude oscillatory shear amplitude measurements (LAOS) techniques [13, 14] and high-speed deformation using a Split Hopkinson pressure bar setup [15]. LAOS tests are usually performed on strain -controlled rheometers with separated motor and transducer [13] to avoid inertial effects.

At rest, STF develop a physically bonded particle network structure [16]. This weak three-dimensional network is due to the stabilization of the particles in solution under electrostatic and Brownian forces, and it is easily broken by stirring the suspension.

The transition from a low to a high viscosity state is associated with a large dissipation of energy [2], which could be exploited in structural applications for damping purposes together with the viscosity increase for stiffness control. Applications proposed towards these properties are integration in dampers [17, 18], in structures such as skis to tailor both their damping and stiffness properties [11, 19] and in personal protective equipment [20, 21]. Flexible ballistic vests known as "liquid armour" [22–24] composed of Kevlar fabrics impregnated with STF have thus been proposed, as well as foam-impregnated STF pads for impact absorption [20, 21]. To use STF in practical applications, it is, however, necessary to control and quantify their damping efficiency. Even though the response of a STF depends very much on the boundary conditions on the fluid, a practical method to quantify and rank several suspensions is based on the evaluation of the energy dissipated per cycle in an oscillatory stress or strain measurement (E_d) for a given suspension. E_d is equivalent to the specific damping energy of the material. This absolute measure of damping is inherent to each material, can be used for modelling purposes, and is a function of temperature, frequency and applied stress.

Measurements of E_d have already been performed for colloidal suspensions [2, 25–27], and calculated as the inner area of a plot of strain versus stress. The curve depicting E_d versus strain amplitude in log–log scale shows two linear regions: one before the transition and one after the beginning of the transition. The slope of the line before the transition was found to be two as expected for linear viscoelastic materials. Yziquel et al. [27] and Kugge and Daicic [25] found an increase of the intercept point with an increase of particle concentration. The slope of the line after the beginning of the transition was reported to be higher than that before the transition [2, 26], which confirms the increase of energy dissipation during shear thickening. Slope values after the transition found in literature are 15 for an aqueous dispersion of spherical silica particles with a diameter of 450 nm at a concentration of about 60 % in volume [2] and 3.97 for a suspension of precipitated calcium carbonate with an average size of 80 nm in PEG200 with a concentration of 40 % in weight [26].

E_d values for STF in literature are reported for one type of colloidal suspension with one particle size, often one concentration and at one frequency. As a result, the influence of the variation of parameters which highly affect the shear thickening response on E_d remains unknown. Furthermore, E_d is given for only a few strain values before the critical strain and after but generally not near the transition. It is thus difficult to apprehend the behaviour of a STF around the critical shear strain or stress.

The present work thus addresses the influence of particle concentration, particle size and frequency on the intrinsic damping properties of STF composed of highly concentrated colloidal suspensions of spherical silica particle in PEG 200. The different steps leading to the calculation of E_d are first presented. E_d curves of STF versus applied strain are compared to those of reference materials used for damping applications. Finally, E_d is used to quantify the damping properties of STF.

Materials

Shear-thickening fluids

Carrier fluid The carrier fluid for all suspensions was a polyethylene glycol with a molecular weight of 200 g mol^{-1}(PEG 200) and a density of 1.12, supplied by Acros Organics. PEG 200 is hydrophilic.

Particles Two different sizes of monodisperse spherical silica particles were provided by Nippon Shokubai Co. Ltd.: KE-P100 with an average diameter of 1 µm and KE-P50 with an average diameter of 500 nm [28].

These particles are manufactured via Stöber synthesis [29]. These hydrophilic particles dispersed in a polar solvent of low molecular weight are shown to result in non-flocculated suspensions [30, 31]. The particles density is 2.

Shear-thickening fluids preparation The PEG 200 and the particles were initially dried 48 h at 60 °C under vacuum to eliminate possible water contamination by the humidity of air. Then, the PEG 200 was added to the particles and hand-mixed to obtain a homogeneous fluid at the desired concentration. Samples were stored in closed jars and immersed in an ultrasonic bath during 3 h at 60 °C to disperse the particles. This complete procedure was shown to provide a fully

dispersed suspension [32, 33]. A list of the STF samples is given in Table 1.

Other materials

By way of comparison, the dissipated energy was measured for several reference samples. Elastomeric materials currently used in vibration control applications were selected in order to compare the STF in terms of damping efficiency. In addition, STF made with fumed silica were investigated as a comparison in terms of polydispersity of the suspension. This easily available STF composition is known to present a smooth shear thickening without discontinuities in opposition to the STF used in the present work.

Smactane® SP is a viscoelastic rubber material developed specially for space applications. Widely used in dampers or damping layers, this material is manufactured by ©SMAC. The density of Smactane is 1.18, and it was received under the form of 2-mm thick sheets. Some of its mechanical and damping properties are reported in [21].

Rhodorsil® RTV-3318 is a soft silicone obtained by polycondensation with a shore hardness of 18 (shore A) which shows good damping properties. The density of silicone is 1.2. silicone disks with a thickness of 1 mm and a diameter of 25 mm were prepared by casting in aluminium moulds. Some of their mechanical and damping properties are reported in [21].

A shear-thickening fluid with polydisperse particles It was constituted of untreated fumed silica and PEG200. The fumed silica particles were Cab-o-sil® M5 from Cabot corporation. These small chains of ø 20- nm silica particles are obtained by flame oxidation of silicon tetrachloride. The specific surface of these particles is 200 $m^2\ g^{-1}$. They are equivalent to Aerosil® 200 fumed silica from Evonik. Their density is similar to that of the monodisperse particles, 2.1. The concentration was set to 20 % *w/w*, which is almost the highest reachable concentration [11]. This sample was prepared and stored using the same protocol as the one used for the monodisperse STF.

Methods

Storage of samples

In order to keep the rheological properties of the shear thickening fluid constant during the test period, all samples were stored in tightly closed jars in a freezer at −24 °C between tests. This was shown in earlier work to be the best method to keep the particles concentration constant overtime, as PEG 200 either evaporates or picks up moisture at room temperature. Controls tests were carried out over the test period to verify that the viscosity of the sample remained the same [33].

Rheological procedures

Rheological tests have all been carried out using an AR2000ex stress controlled rheometer from TA instruments. The tests were carried out in a room with controlled temperature at 23 ± 1 °C. Parallel plates [2, 34, 35] of 25-mm diameter were used, with a gap of 800 µm for the STF, 2 mm for the Smactane® and 1 mm for the silicone. In order to avoid the wall slip between the sample and the plates, the plates surfaces were covered with sandpaper P220 (grain size of 68 µm) glued with a cyanoacrylate glue as recommended in the literature [2, 36]. Cone-plate geometry was not used for this reason. The gap value was selected as no change of viscosity was observed in a gap range of 800 ± 300 µm.

Before inserting the samples between the plates, the STF were vigorously hand mixed to destroy any potential physically bonded particle network formed at rest. The samples then stayed at rest during 2 min, to break-up the hydroclusters possibly formed by shear during the deposition of the samples.

Two series of tests were carried out to characterize the samples:

Steady state flow measurements They provide basic information on the shear thickening properties of a fluid such as the increase of viscosity η during the transition and the kinetics of this transition. The shear rate was varied from

Table 1 Flow characteristics of the monodisperse STF

Ref. particle	Solid fraction [Percent *w/w*]	Viscosity [Pa s] at 10^{-2} s	Minimal viscosity [Pa s]	Maximal viscosity [Pa s]	Viscosity increase [%]	Critical shear rate [s^{-1}]	Normal force max [*N*]
KE-P50	68.00 ± 0.05	190 ± 20	22 ± 2	36,000 ± 2,000	1,600 ± 200	0.48 ± 0.08	4.66 ± 0.76
KE-P50	67.50 ± 0.05	47 ± 16	5.2 ± 1.2	1,400 ± 700	290 ± 170	2.9 ± 2.0	0.69 ± 0.28
KE-P50	67.00 ± 0.05	35 ± 7	1.2 ± 0.4	190 ± 15	15.4 ± 1.7	9.8 ± 2.8	0.54 ± 0.07
KE-P100	68.00 ± 0.05	31,00 ± 1,700	72.2 ± 8.5	150,000 ± 40,000	2,200 ± 800	0.075 ± 0.004	17.22 ± 11.61
KE-P100	66.80 ± 0.05	64 ± 15	8.5 ± 1.0	8,800 ± 1,300	1,000 ± 200	0.68 ± 0.18	0.50 ± 0.38

0.01 to 100 s^{-1} during the tests with increasing angular velocity, with 20 points per decades, and a maximum measurement time of 1 min and 30 s per point with a sampling time of 15 s. This compromise was defined to best capture the critical shear stress value, while keeping the duration of the experiment under 1 h.

Oscillation tests These tests are performed to calculate the energy dissipated by the STF. They consist in a oscillatory stress ramp from 0.1 to 60,000 Pa applied to the sample. Each stress step was constituted of a conditioning time of 5 s and a sampling time of 5 s. This kind of test was conducted at four different frequencies for each sample: 0.1, 0.5, 1 and 2 Hz. For each oscillatory test, control parameters such as the raw phase angle and the oscillatory torque were checked to ensure that they stay within the validity of the rheometer corrections, which was not the case above 2 Hz. Each test was repeated three times with a new sample of the same composition to check for reproducibility.

Methodology to calculate E_d

Theory The energy dissipated during one cycle corresponds to the mechanical work due to stress applied to the sample for each cycle. The dissipated energy per cycle E_d is:

$$E_d = \Delta W = \int \tau d\gamma = \int_0^{\frac{2\pi}{\omega}} \tau \frac{d\gamma}{dt} dt \quad (1)$$

Where W is the work, τ the shear stress, γ the shear strain and ω the angular frequency [37].

In our experiments, the dissipated energy was obtained by integrating the area of the hysteresis contained in a plot of stress versus strain during a dynamic oscillatory test [2, 25, 27]. In the case of harmonic signals, this plot can be represented with a Lissajous plot. The hysteresis is due to the phase shift between the stress and the strain. For a linear viscoelastic material the Lissajous plot is a perfect ellipse.

Raw data extraction To plot a Lissajous curve, stress and strain values for one cycle of oscillation at a defined frequency and stress value are extracted from the raw data of a stress sweep test. The raw data, oscillatory torque and radial displacement are converted to more usual oscillatory and strain values. Before the transition, STF typically behave like a viscoelastic material: the solicitation (oscillatory torque) and the response (radial displacement) are perfect sinusoids with a phase shift between 0 and 90 ° as shown in the first graph of Fig. 1. After the transition, the response is distorted and takes a rectangular shape near the transition and a distorted sinusoid shape far from it. This typical evolution of the response signal with an increase of the stress amplitude has been previously reported in the literature [13, 27, 38]. The rectangular shape reveals the non-linear response of shear thickening, as the experimental signal is composed of several harmonics [27]. In our case, it was not possible to extract

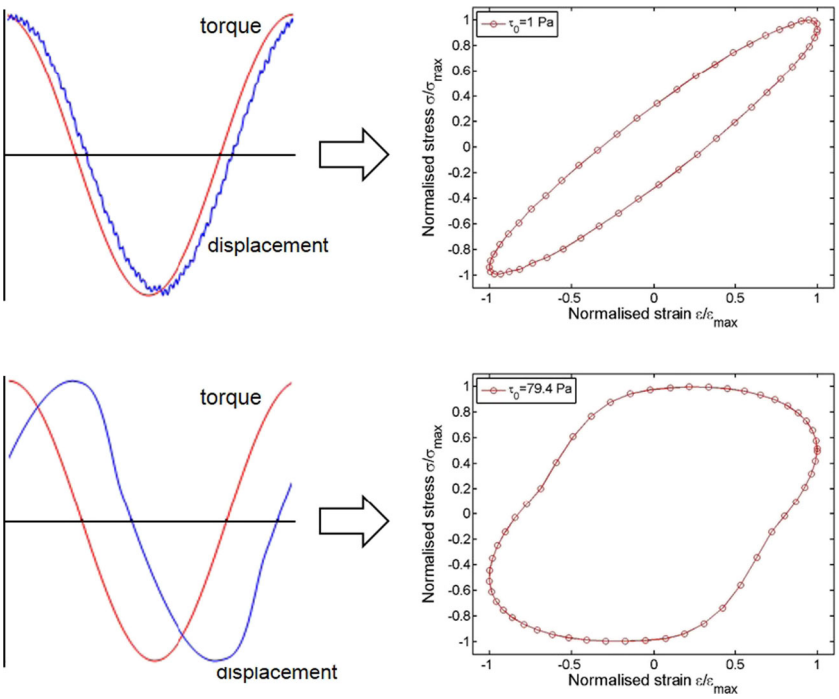

Fig. 1 Extraction of Lissajous curve from the raw data of a stress sweep test conducted on a KE-P50/PEG 200 c. 68 % *w/w* at 1 Hz

complete LAOS data such as the odd harmonics through Fourier transform of the data, due to the rather low sampling rate inducing large signal to noise ratio [13]. The non-linear aspects are instead taken into account through the integration of the distorted shapes directly from the Lissajous curves.

Experimental results

Flow viscosity

Figure 2 presents rheograms obtained during the flow tests of STF with KE-P50 particles. The flow viscosity is plotted in function of the shear rate. All samples show a discontinuous shear-thickening effect, with a drastic viscosity increase at a critical shear rate value. Table 1 summarizes all results in terms of initial viscosity, minimal and maximal viscosity, critical shear rate and the maximal normal force recorded during the transition, which reflects the dilatancy of the suspension. In agreement with literature [1, 11], we observed that an increase in concentration (Fig. 2a) resulted in:

- a higher viscosity during the shear thinning phase preceding the shear thickening,
- a lower critical shear rate characterizing the start of the shear thickening phenomenon,
- a higher viscosity peak value reached during shear thickening, although this is difficult to capture in the case of a discontinuous transition.

Figure 2b shows the influence of the particle size. In colloidal suspensions (ø < 1 µm), the critical shear rate decreases with an increase in particle size, as previously reported [1].

The increase in viscosity due to shear thickening is higher for monodisperse particles than for polydisperse (fumed silica) as pictured in Fig. 2b, from 1 to 3 orders of magnitude for polydisperse STF and 2 to 4 for monodisperse STF.

Stress sweep tests

Figure 3 presents the results for the oscillatory stress sweep tests on the STF with KE-P50 particles. For a greater ease of understanding, the norm of the complex viscosity $\eta^* = \sqrt{\eta'^2 + \eta''^2}$ is shown in the function of the strain amplitude instead of the stress amplitude. The critical strain decreases and inversely the critical stress increases with an increase of frequency. As expected for dynamic measurements on concentrated suspensions, a Newtonian plateau is first observed at low shear, followed by a shear thinning phase and then the shear thickening phase [2, 39].

As the sample is manually inserted on the rheometer plates, the viscosity at the beginning of the test slightly differs between samples. The formation of a partial physically bonded particle network in the sample, however, exerts only a small influence on the value of the critical strain or stress, by decreasing them slightly. It affects the behaviour of the STF only at low strains before the shear thickening which then causes larger changes in the microstructure.

In colloidal suspensions of silica particles, the shear thickening phenomenon is reversible and the return to the initial state takes place in only a few seconds [9, 16]. Hysteresis is negligible [10, 28]. For two successive stress sweep tests performed on the same sample, the results are similar save for the viscosity at the beginning of the test which can change in function of the particle network structure at rest, in the range of 5 to 20 Pa s.

Energy dissipated per cycle for a monodisperse shear thickening fluid in PEG200

Lissajous plot Examples of Lissajous plots obtained from a stress sweep test are presented in Fig. 4. The Lissajous plots evolve from an ellipsoid to an oblong shape after the transition, as shear thickening is a non-linear phenomenon. At high stress levels, above 100 Pa, the Lissajous curves

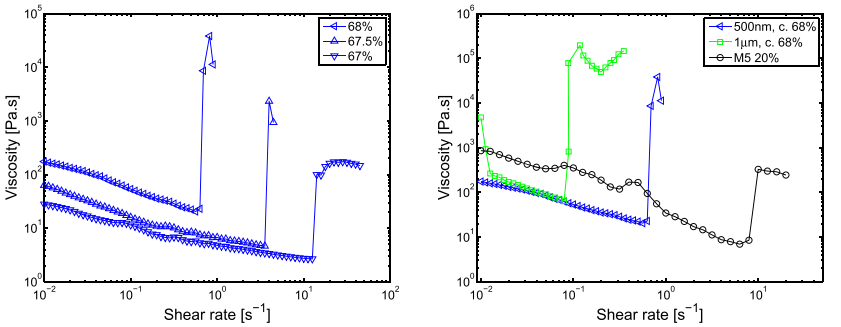

(a) KE-P50 $\varnothing 500\,nm$

(b) Monodisperse particle size $\varnothing 0.5$ and $1\,\mu m$ and fumed silica

Fig. 2 Viscosity of monodisperse spherical silica particles and fumed silica concentrated suspensions in PEG200 for various particle size and concentration in *w/w*

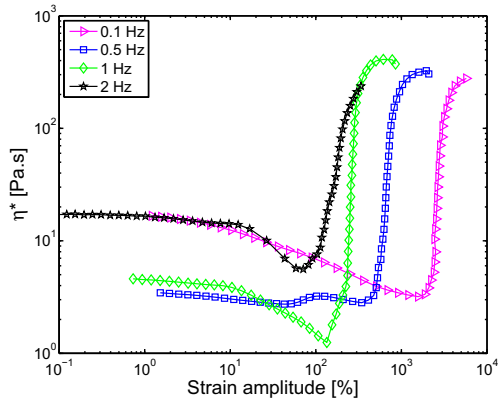

Fig. 3 Decrease of the critical strain amplitude with an increase in frequency for KE-P50/PEG 200(c. 67 % *w/w*) STF

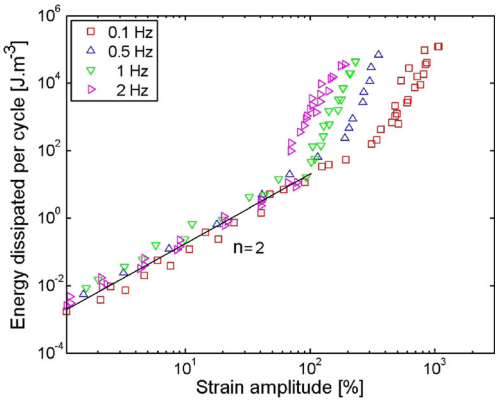

Fig. 5 Energy dissipated per cycle of a STF KE-P50/PEG 200 c. 67.5 % *w/w* at 0.1, 0.5, 1 and 2 Hz

become distorted ellipsoids. The relative area of the distorted ellipsoids thus tends to decrease with stress level. This is in opposition with the expected behaviour [2], nonetheless this phenomenon has already been reported in literature [38], and attributed to flow blockage.

Dissipated energy Figure 5 plots E_d calculated using Eq. 1 in function of the strain amplitude reached during each solicitation cycle. A detailed explanation of the method used to calculate E_d is given in section "Methodology to calculate E_d". A linear increase in log–log scale is observed on the curve before the critical strain, where E_d values for different frequencies all follow the same behaviour (Fig. 5). For values above the critical strain, the E_d values also follow a linear behaviour in log–log scale, which also depends on frequency (Fig. 5).

An increase in frequency tends to increase the dissipated energy, in particular after the transition (Fig. 5). The velocity of the sliding friction mechanisms between the fluid and the particles increases with frequency, so does the Coulomb damping which corresponds to the dissipation of energy by friction.

Critical strain Critical strains were taken as the intersection of the dissipated energy curves before and during the transition. These data are similar to, yet more precise than the values directly extracted from the raw rheological data. The critical strain decreases when frequency increases (Fig. 6) as previously reported in literature [2, 19]. This is crucial for potential applications, for which it will be possible to activate the STF with much lower strains when the frequency is higher. The critical strain and stress also decrease when particle concentration increases.

Influence of the formation of a physically bonded particle network prior to the test The initial viscosity of the STF at rest is correlated to the extent of the formation of a physically bonded particle network. In all our rheological experiments, we break the structure formed at rest and use a pre-shear to ensure reproducible results. We nonetheless carried out one test experiment where we simulated a practically relevant condition, with the STF initially at rest for a long time, forming the physical network, then sheared during an event. Figure 7 compares two test results of the same fluid: in one case, the particle network structure formed at

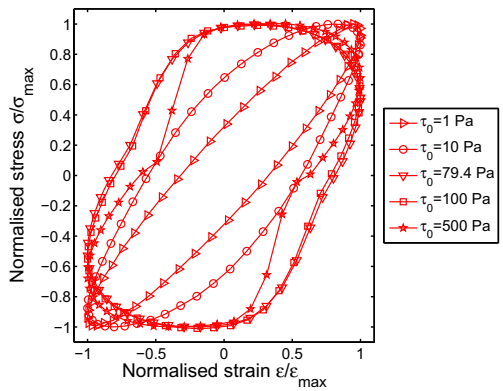

Fig. 4 Scaled Lissajous plots for a STF KE-P50/PEG 200 c. 68 % *w/w* at 1 Hz, the transition begins at an oscillatory stress of 79.4 Pa

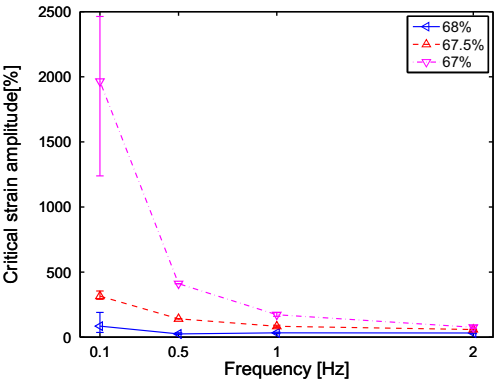

Fig. 6 Critical strain for a STF KE-P50/PEG 200 at various concentrations *w/w* in function of frequency

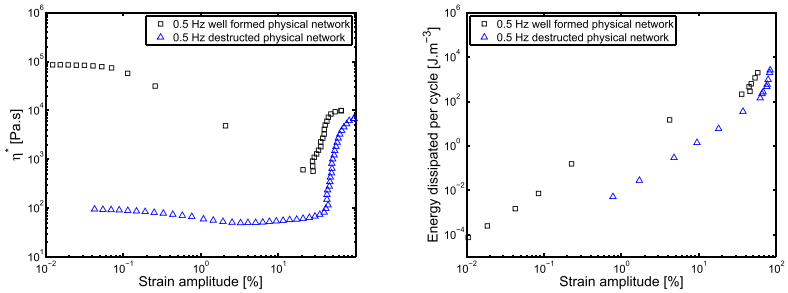

Fig. 7 Influence of the particle network formed during rest on E_d for a STF KE-P50/PEG 200 c. 68 % *w/w* at 0.5 Hz

(a) Influence of the particle network formed during rest on complex viscosity during a stress sweep test

(b) E_d with or without a particle network formed during rest

rest was preserved as much as possible during the transfer of the STF from the storage container to the rheometer; in the other case, the STF was hand-mixed to break the physical network structure before the experiment. Both η^* (Fig. 7a) and E_d (Fig. 7b) before the transition are higher for the test with the preserved particle network structure. This network thus increases the *y*-intercept of the lines describing the E_d. The energy results presented in this article thus constitute a lower bound of the levels that could be attained, if activation takes place intermittently.

Influence of particle concentration E_d curves for different concentrations of KE-P50 (ø 500 *nm*) particles in PEG 200 are shown in Fig. 8 at different frequencies. The E_d of the reference samples (silicone Rhodorsil® RTV-3318 and Smactane®) are plotted along for comparison purposes.

The increase in particle concentration leads to an increase of E_d as reported in Fig. 8, both before and during the transition. This is attributed to the increased friction between neighbouring particles, since particles are forced to be closer overall. Increasing particle concentration can thus constitute a method to increase the damping properties of STF. However the processing range regarding particle concentration is very limited as shown in Fig. 2a. The critical shear rate that marks the beginning of the transition decreases with an increase in particle concentration, and the material becomes impractical to handle at high concentrations.

Influence of the particle size E_d increases when the particle size is smaller, for the highly concentrated suspensions of monodisperse silica particles in PEG 200 as shown in Fig. 9.

With the decrease of the particle size by a factor 2, for a same volume fraction there will be 8 times more particles in suspension. More particles lead to more contact area between the fluid and the particles and more friction damping between the fluid and the particles.

Comparison with other reference materials The behaviour of the Smactane and of the silicone correspond to that of a linear viscoelastic material, a straight line with a slope of 2 as shown in Eq. 3 (Fig. 8). Comparing the STF with the benchmark materials, the latter present better damping properties than STF as shown in Fig. 8 before the transition, whatever the particle size, with the exception of the STF KE-P50/PEG 200 with a concentration of 68 % *w/w* above 0.5 Hz that possesses almost the same E_d as the silicone. During the transition, the E_d curves of all STF cross the prolongation of the silicone E_d curve. This indicates that the STF at this stage shows better damping properties than the silicone in terms of dissipated energy per cycle. The only case for which the STF may overcome the Smactane®

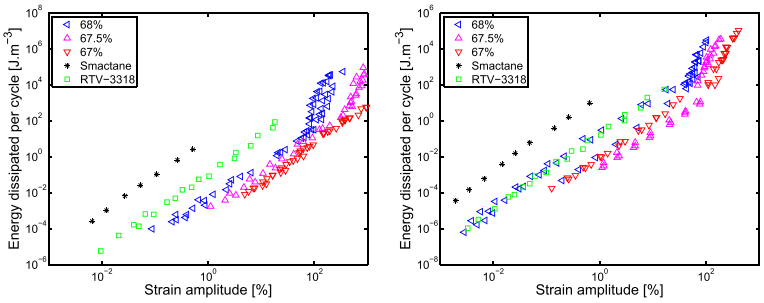

Fig. 8 E_d for STF KE-P50/PEG 200 at different particle concentration in *w/w*, Smactane and Rhodorsil RTV-3318 at 0.1 and 2 Hz

(a) 0.1 Hz

(b) 2 Hz

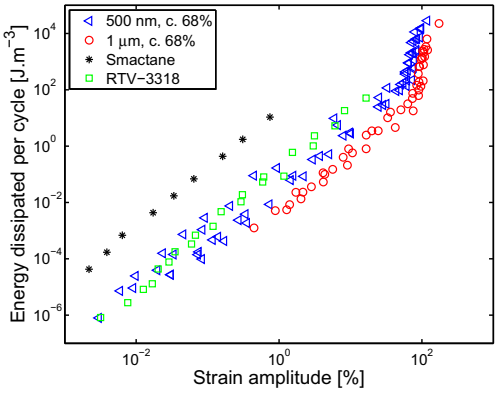

Fig. 9 E_d for highly concentrated shear thickening suspension of monodisperse silica particles with different particle size (KE-P100 = 1 µm, KE-P50 = 500 nm) , Smactane and RTV-3318 at 1 Hz

in damping efficiency would be potentially for very large strain amplitude.

Quantification of the STF damping properties using the dissipated energy per cycle

The dissipated energy per cycle E_d was defined using Eq. 1. The E_d curve plot in log–log scale shows two linear behaviours before and after the critical shear strain. E_d can thus be written as [40]:

$$E_{\mathrm{d\,pre}} = J_{\mathrm{pre}} \cdot \gamma_0^{n_{\mathrm{pre}}} \quad \text{and} \quad E_{d\,\mathrm{during}} = J_{\mathrm{during}} \cdot \gamma_0^{n_{\mathrm{during}}} \quad (2)$$

Where J is a constant related to the dissipative modulus, corresponding to the value of Energy found for $\gamma_0 = 1$, n is the damping exponent, γ_0 is the strain amplitude for a given cycle of solicitation. *pre* correspond to the value before the critical shear stress and *during* to the value during the transition.

The n values measured on the plots are all close to two before the transition for all the materials investigated. This confirms that they behave like a viscoelastic material [41], for which

$$E_{\mathrm{d\,visco}} = \pi \cdot G'' \cdot \gamma^{2_{\mathrm{pre}}} \quad (3)$$

No clear trend appears with frequency or particle concentration for the n values after the transition, they all remain within the range of 7 to 14, in in agreement with values previously reported in the literature [23], i.e., much higher than in the pre-transition region. The J values fluctuate greatly before and during the transition. Nonetheless, since during the transition, the values of the slope consistently increase from 2 to between 6 and 15 as shown in Fig. 5, this indicates that STF dissipate energy more efficiently during the transition than initially, where it behaves as a linear viscoelastic fluid.

Conclusion

This work analysed the role of frequency, particle concentration and size on the dissipated energy E_d of highly concentrated suspensions of STF constituted of monodisperse spherical particles of silica in PEG 200.

STF consistently behaved like a linear viscoelastic material before the transition as the slope n of the E_d curve was two. During the transition, the dissipated energy increased, with n values between 7 and 14 for this type of suspension.

The dissipated energy per cycle increased with frequency and particle concentration and decreased with particle size. The formation of a particle network during rest in the colloidal suspension also contributed to a small increase of the E_d before and during the transition, which could become significant if the material is fully at rest before use.

Finally, we observed that in specific cases of high shear at low frequency, STF may dissipate more energy than traditional damping elastomers. As reported elsewhere, the same behaviour should be expected with the increase of frequency, as the critical amplitude decreases inversely with the frequency and eventually reach a plateau [11]. STF could thus find specific applications where a two-step behaviour would be beneficial, such as for impact protection in shoes or seismic dampers[21].

To complete the study, an investigation using the LAOS technique would lead to a greater understanding of the nonlinear effects in shear-thickening behaviour; however, first conclusions were reached to select the best compromise in concentration and particle size for a given application. Smaller particles at high concentrations would lead to the fastest and highest response, in particular at higher frequencies, and the presence of a particle network structure seems to be beneficial, although it cannot be guaranteed for fast activation cycles. Tests at higher frequency range would complement these conclusions, for example, using dynamic mechanical analysis or a vibration test of a model structure.

Acknowledgments The European Space Agency Networking/ Partnering Initiative (NPI) is gratefully acknowledged for financial support. V. Eberlé is thanked for her contribution to this work during her studies.

References

1. Barnes HA (1989) Shear-thickening (dilatancy) in suspensions of nonaggregating solid particles dispersed in newtonian liquids. J Rheol 33(2):329–366
2. Lee YS, Wagner NJ (2003) Dynamic properties of shear thickening colloidal suspensions. Rheol Acta 42(3):199–208
3. Bertrand E, Schmitt V, Bibette J (2002) From shear thickening to shear-induced jamming. Phys Rev E 66:060401

4. Brown E, Heinrich MJ (2012) The role of dilation and confining stresses in shear thickening of dense suspensions. J Rheol 56(4):875–923
5. Chaffey C (1977) Mechanisms and equations for shear thinning and thickening in dispersions. Colloid Polym Sci 255(7):691–698
6. Bossis G, Brady JF (1989) The rheology of Brownian suspensions. J Chem Phys 91:1866–1874
7. Bergenholtz J, Brady JF, Vicic M (2002) The non-Newtonian rheology of dilute colloidal suspensions. J Fluid Mech 456:239–275
8. Bender JW, Wagner NJ (1995) Optical measurement of the contributions of colloidal forces to the rheology of concentrated suspensions. J Colloid Interface Sci 172(1):171–184
9. Bender JW, Wagner NJ (1996) Reversible shear thickening in monodisperse and bidisperse colloidal dispersions. J Rheol 40(5):899–916
10. Maranzano BJ, Wagner NJ (2001) The effects of interparticle interactions and particle size on reversible shear thickening: Hard-sphere colloidal dispersions. J Rheol 45(5):1205–1222
11. Fischer C, Bennani A, Michaud V, Jacquelin E, Månson J-A (2010) Structural damping of model sandwich structures using tailored shear thickening fluid compositions. Smart Mater Struct 19(3):035017 (7 pp)
12. Saito Y, Hirose Y, Otsubo Y (2012) Size effect on the rheological behavior of nanoparticle suspensions in associating polymer solutions. Colloid Polym Sci 290(3):251–259
13. Hyun K, Wilhelm M, Klein CO, Cho KS, Nam JG, Ahn KH, Lee SJ, Ewoldt RH, McKinley GH (2011) A review of nonlinear oscillatory shear tests: analysis and application of large amplitude oscillatory shear (laos). Prog Polym Sci 36(12):1697–1753
14. Onogi S, Masuda T, Matsumoto T (1970) Non-linear behavior of viscoelastic materials. I. Disperse systems of polystyrene solution and carbon black. Trans Soc Rheol 14(2):275–294
15. Lim AS, Lopatnikov SL, Wagner NJ, Gillespie JW (2011) Phenomenological modeling of the response of a dense colloidal suspension under dynamic squeezing flow. J Non-Newtonian Fluid Mech 166(12-13):680–688
16. Galindo-Rosales FJ, Rubio-Hernández FJ, Velázquez-Navarro J (2009) Shear-thickening behavior of aerosil r816 nanoparticles suspensions in polar organic liquids. Rheol Acta 48(6):699–708
17. Helber R, Doncker F, Bung R (1990) Vibration attenuation by passive stiffness switching mounts. J Sound Vib 138(1):47–57
18. Zhang XZ, Li WH, Gong XL (2008) The rheology of shear thickening fluid (stf) and the dynamic performance of an stf-filled damper. Smart Mater Struct 17(3):035027
19. Neagu RC, Bourban P-E, Månson J-AE (2009) Micromechanics and damping properties of composites integrating shear thickening fluids. Compos Sci Technol 69(3-4):515–522
20. Dawson MA, McKinley GH, Gibson LJ (2009) The dynamic compressive response of an open-cell foam impregnated with a non-Newtonian fluid. J Appl Mech 76(6):061011
21. Soutrenon M, Michaud V (2014) Impact properties of shear thickening fluid impregnated foams. Smart Mater Struct 23(3):035022
22. Decker MJ, Halbach CJ, Nam CH, Wagner NJ, Wetzel ED (2007) Stab resistance of shear thickening fluid (stf)-treated fabrics. Compos Sci Technol 67(3-4):565–578
23. Lee YS, Wetzel ED, Wagner NJ (2003) The ballistic impact characteristics of kevlar woven fabrics impregnated with a colloidal shear thickening fluid. J Mater Sci 38(13):2825–2833
24. Trigg C, Dyke A, Davies J, Dunleavy M (2011) Impact studies of shear thickening fluids incorporated within composite structures. Int J Mater Eng Innov 2(2):136–148
25. Kugge C, Daicic J (2004) Shear response of concentrated calcium carbonate suspensions. J Colloid Interface Sci 271(1):241–248
26. Yang H, Ruan J, Zou J, Wu Q, Zhou Z, Xie Y (2009) Non-linear viscoelastic rheological properties of pcc/peg suspensions. Chin J Chem Phys 22(1):46–50
27. Yziquel F, Carreau PJ, Tanguy PA (1999) Non-linear viscoelastic behavior of fumed silica suspensions. Rheol Acta 38:14–25
28. Kalman DP, Wagner NJ (2009) Microstructure of shear-thickening concentrated suspensions determined by flow-usans. Rheol Acta 48(8):897–908
29. Stober W, Fink A, Bohn E (1968) Controlled growth of monodisperse silica spheres in the micron size range. J Colloid Interface Sci 26(1):62–69
30. Raghavan SR, Hou J, Baker GL, Khan SA (2000) Colloidal interactions between particles with tethered nonpolar chains dispersed in polar media: direct correlation between dynamic rheology and interaction parameters. Langmuir 16(3):1066–1077
31. Raghavan SR, Walls HJ, Khan SA (2000) Rheology of silica dispersions in organic liquids: New evidence for solvation forces dictated by hydrogen bonding. Langmuir 16(21):7920–7930
32. Hassan TA, Rangari VK, Jeelani S (2010) Sonochemical synthesis and rheological properties of shear thickening silica dispersions. Ultrason Sonochem 17(5):947–952
33. Soutrenon M, Michaud V, Månson J-AE (2013) Influence of processing and storage on the shear thickening properties of highly concentrated monodisperse silica particles in polyethylene glycol. Appl Rheol 23:54865
34. Brown E, Forman NA, Orellana CS, Zhang H, Maynor BW, Betts DE, Desimone JM, Jaeger HM (2010) Generality of shear thickening in dense suspensions. Nat Mater 9(3):220–224
35. Fischer C., Braun SA, Bourban P-E, Michaud V, Plummer CJG, Månson J-A (2006/10/) Dynamic properties of sandwich structures with integrated shear-thickening fluids. Smart Mater Struct 15(5):1467–75
36. Fischer C (2007) Adaptive composite structures for tailored human–materials interaction. PhD thesis, EPFL
37. Macosko C (1994) Rheology: principles, measurements, and applications. Advances in interfacial engineering series, Wiley
38. Boersma WH, Laven J, Stein HN (1992) Viscoelastic properties of concentrated shear-thickening dispersions. J Colloid Interface Sci 149(1):10–22
39. Fischer C, Plummer CJG, Michaud V, Bourban P-E, Månson J-AE (2007) Pre- and post-transition behavior of shear-thickening fluids in oscillating shear. Rheolog Acta 46:1099–1108
40. Yziquel F, Carreau PJ, Moan M, Tanguy PA (1999) Rheological modeling of concentrated colloidal suspensions. J Non-Newtonian Fluid Mech 86(1-2):133–55
41. Lakes R (2009) Viscoelastic materials. Cambridge University Press